

Aggregation Behavior of Protoporphyrin IX in Aqueous Solutions: Clear Evidence of Vesicle Formation

Luigi Monsù Scolaro,^{*,†,‡} Mariangela Castriciano,[†] Andrea Romeo,[†] Salvatore Patanè,^{‡,§} Eugenio Cefali,^{‡,§} and Maria Allegrini[#]

Dipartimento di Chimica Inorganica, Chimica Analitica e Chimica Fisica, Università di Messina, and Istituto di Chimica dei Prodotti Naturali (ICTPN-CNR), Sezione di Messina, Messina, Italy, INFN, Unità di Messina, Messina, Italy, Dipartimento di Fisica della Materia e Tecnologie Fisiche Avanzate, Università di Messina, Messina, Italy, and INFN and Dipartimento di Fisica, Università di Pisa, Pisa, Italy

Received: August 15, 2001; In Final Form: December 17, 2001

The aggregation behavior of protoporphyrin IX in aqueous solution, as a function of pH and ionic strength, has been studied by means of UV/vis, fluorescence emission spectroscopy, and resonant light scattering (RLS) techniques. Our experimental results agree with previous literature assignments: (i) protoporphyrin IX is a monomer in the pH range 0–3, (ii) a dimer is present for pH > 8, and (iii) higher aggregates are present in the pH range 3–7. Addition of sodium chloride up to 0.3 M to a porphyrin solution at pH 12 gives a process resembling a phase transition, whereas it has little effect on acidic or neutral solutions. The apparent split Soret band observed in the intermediate pH range has been explained using a model in which dimers of porphyrins (with a slip angle $\alpha = 38^\circ$ or 52° , as derived from depolarized RLS measurements) are the basic units and they interact axially through π – π stacking and laterally by edge-to-edge hydrophobic contacts. The half neutralization of the carboxylic acid side chains is responsible for the occurrence of a network of intermolecular hydrogen bonds, which contribute to a better stabilization of the supramolecular assembly. Evaporation on a glass surface of solutions containing protoporphyrin IX aggregates from samples at intermediate pH leads to aggregates stable enough to be investigated for the first time through scanning electron (SEM) and scanning near-field optical microscopy (SNOM). These species evidence a prolate shape with an average size of 200–500 nm and a medium height of 60 nm, which is in agreement with the hydrodynamic radii as measured in solution by dynamic light scattering. On consideration of the amphiphilic character of protoporphyrin IX, these observations suggest the formation of multilamellar or onion-like vesicles. The analysis of the SNOM images points to the presence of regions in which the aggregation process resulted in a thin film covering the vesicles. An analysis of SEM experiments reveals also the contemporary presence of large regions in which the vesicles collapse in a continuum layered structure.

Introduction

Porphyrin aggregation through the occurrence of π – π stacking interactions is a well-known phenomenon for this class of compounds.^{1,2} Protoporphyrin IX (Figure 1) is the iron-free form of hemin, one of the most common natural porphyrins. This compound should exhibit amphiphilic properties, forming vesicles and molecular bilayers, because of the contemporary presence of two peripheral ionizable propionate groups and a large hydrophobic surface.³ Such a molecule, in alkaline aqueous solutions, is expected to lead to stable face-to-face dimers with a head-to-tail disposition of the charged carboxylate groups. Extended supramolecular structures can be also formed because of the occurrence of a hydrogen-bonding network between the partially neutralized carboxylic acid side chains at intermediate pH values. Indeed, this latter property has been fully investigated

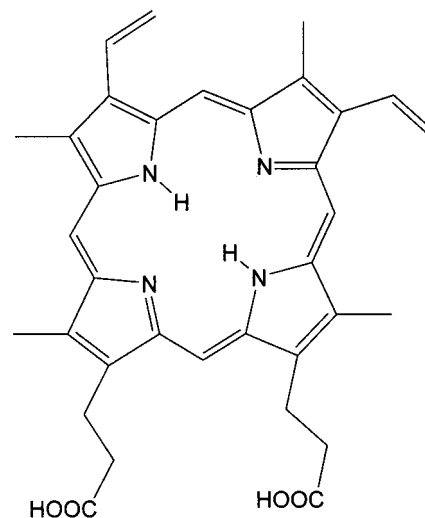


Figure 1. Protoporphyrin IX.

and verified only in the case of properly designed protoporphyrin IX derivatives. Long-lived and light stable micellar fibers, stabilized through hydrogen bonding and hydrophobic interactions, were obtained from bis-glycosamide derivatives.⁴ The

* To whom correspondence should be addressed. Dipartimento di Chimica Inorganica, Chimica Analitica e Chimica Fisica, Università di Messina, Salita Sperone 31, 98166 Vill. S. Agata, Messina, Italy. Telefax: +39-090-393756. E-mail: monsu@chem.unime.it.

[†] Università di Messina, and Istituto di Chimica dei Prodotti Naturali (ICTPN-CNR).

[‡] INFN.

[§] Università di Messina.

[#] Università di Pisa.

polymeric ribbonlike structure was modeled on the basis of a porphyrin octamer in which face-to-face and strong edge-to-edge interactions are mainly responsible for the observed apparently split Soret band. Diamino-substituted protoporphyrin IX derivatives lead to micellar rods and vesicular tubules, of which the stability is strongly pH-dependent.⁵ Amphiphilic tin(IV) porphyrinate dichloride derivatives form micellar fibers in which a lateral arrangement of porphyrins occurs via axial hydrogen chloride ligands acting as facial groups.⁶

Despite the importance of protoporphyrin IX, its aggregation behavior has not been investigated in great detail. After an early report on the monomer–dimer equilibrium,⁷ the solubilization of protoporphyrin IX⁸ and of the corresponding hemin in Triton X-100 micelles as monomeric species⁹ and the interaction with water-soluble PVP polymer have been reported.¹⁰ The photo-physical behavior has been studied only in micellar phases,¹¹ and the experimental findings suggested an equilibrium distribution of porphyrin near the surface of the micelles. Controversial results deal with the nature and the stability of the species present in aqueous solution as function of pH. Inamura et al.,¹⁰ using a combination of UV/vis spectroscopy and size-exclusion gel chromatography, pointed to the presence of monomeric ($\lambda_{\text{max}} = 405$ nm) and dimeric ($\lambda_{\text{max}} = 388$ nm) porphyrin at pH 1 and 12, respectively. Under mild acidic conditions (pH 4.8), they reported the formation of extended aggregates (MW > 700 000 Da), characterized by a split Soret band displaying components at longer and shorter wavelengths with respect to the monomer. Other authors reported just the presence of a shoulder at 460 nm under neutral pH conditions, while rapid precipitation occurs on decreasing pH.⁴ Results similar to those of Inamura et al. were obtained only by using water/dimethyl sulfoxide mixtures (1:20 in molar ratio) as solvent. Anyway, the instability and low reproducibility of the experimental results prevented further investigations.

On these bases, we thought it worthwhile to study the colloidal behavior of this porphyrin through of a combination of spectroscopic techniques. In particular, we used resonance light scattering (RLS), which has been successfully exploited as a sensitive and selective probe of the electronic and geometrical properties of aggregated chromophores, such as porphyrins^{12–14} and chlorophyll *a*.¹⁵ The RLS effect arises from an enhancement of the scattered light intensity in close proximity of an absorption band, allowing for the identification of aggregated chromophores, even in complex matrixes. The occurrence of this phenomenon is related to (i) strong electronic coupling between adjacent chromophores, (ii) the size and geometry of the resulting aggregate, and (iii) the intense molar extinction of the monomeric constituents.^{12,14} A simple quantum mechanical model for RLS based on exciton-coupling theory has been recently developed, addressing the relationship between the intensities of the observed RLS features and the electronic and geometrical properties of the aggregates.¹⁶

We report also the first scanning electron (SEM) and scanning near-field optical microscopy (SNOM) investigation pointing clearly out that protoporphyrin IX forms vesicles in aqueous solutions under weak acidic conditions.

Materials and Methods

Preparation of Aggregates. Protoporphyrin IX was purchased from Aldrich as disodium salt. Its purity was checked through ¹H NMR spectroscopy in dms-*d*₆. Stock solutions of the porphyrin were prepared by weighing a known amount of solid and dissolving it in dimethyl sulfoxide (Aldrich, spectral grade). These solutions were stored in the dark and used within a week.

A proper amount of this solution was diluted in Milli-Q water, previously filtered through a 0.2 μm syringe filter to remove dust, and the pH was adjusted by adding HCl or NaOH. In all experiments, the concentration of dimethyl sulfoxide in water was less than 5% (v/v).

Spectroscopic Measurements. UV/vis spectra were obtained on a Hewlett-Packard model HP 8453 diode array spectrophotometer. Fluorescence emission and resonance light scattering (RLS) experiments were performed on a Jasco model FP-750 spectrofluorimeter, adopting in the latter case a synchronous scan of both the excitation and emission monochromator with a right-angle geometry.^{12,14} Depolarized resonance light scattering measurements were obtained on the same instrument equipped with linear polarizers (Sterling Optics 105UV). The depolarization ratio is defined as $\rho_V(90) = I_{VH}/I_{VV}$, where I_{VH} and I_{VV} are the scattered light intensities with horizontal and vertical polarization, respectively. The different transmission efficiency of polarized light by both excitation and emission monochromators has been accounted for by correcting the I_{VH} value through the following equation: $\rho_V(90) = G \cdot I_{VH}/I_{VV}$, where $G = I_{HV}/I_{HH}$ is a correction factor.¹⁶

Dynamic light scattering measurements (DLS) were performed on a Malvern 4700 submicron particle analyzer. The exciting light source was a 17 mW polarized HeNe laser (632.8 nm).

Microscopy. Protoporphyrin IX aggregates for the microscopy analyses were deposited on glass cover slides from an aqueous solution at pH 5 and dried under a gentle nitrogen stream. SEM analysis was performed on a LEO S420 Cambridge instrument operating with an accelerating potential of 20 kV. The samples were prepared by graphite coating.

Further information on morphology and optical properties of the sample were obtained by means of scanning near-field optical microscopy (SNOM). This technique is very powerful because it is able to overcome the diffraction limit with a lateral resolution well below 100 nm.^{17,18} A near-field optical probe acts as a subwavelength light source, which is scanned in close proximity over the sample surface. Near-field microscopy is a true scanning probe method, which provides simultaneously optical and topographic information.

SNOM measurements were performed by means of a “homemade” aperture microscope in excitation mode configuration.^{19,20} The instrument was operating in constant gapwidth mode (CGM) stabilizing the distance between the sample and the tip by a standard optical shear-force detection method.^{21,22} The near field is provided by a solid-state laser emitting at 635 nm and coupled to a commercially available tapered optical fiber (Nanonix) with an aperture of 50 nm. Because of the features of the technique, namely, super resolution and room condition working capability, the sample was observed “as it is” after the deposition, that is, without any pretreatment or preserving of, in such a way, its topographic and optical properties. Measurements were performed with a scan rate of about 12 nm/min and a sampling of 256 point/row. Optical and topographic data were simultaneously collected during the scans and stored in a personal computer for further analysis.

Results

Protoporphyrin IX is readily solubilized in dimethyl sulfoxide and the corresponding UV/vis spectrum exhibits an intense Soret band at 408 nm ($\epsilon = 1.7 \times 10^5 \text{ M}^{-1} \text{ cm}^{-1}$), together with four weaker Q-bands at 506, 542, 577, and 630 nm. The effect of changing pH has been investigated in the range 1–12. Figure 2 shows the spectroscopic features of aqueous porphyrin

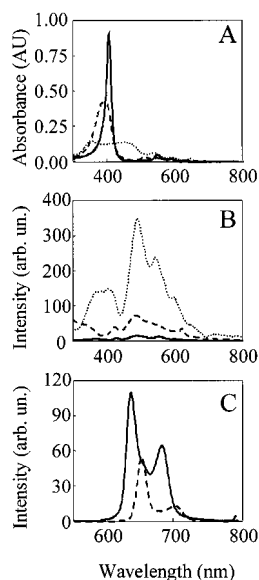


Figure 2. UV/vis (A), RLS (B), and fluorescence emission (C) spectra of a 5 μM aqueous solution of protoporphyrin IX under different pH conditions: pH = 1 (solid line), pH = 4.8 (dotted line), and pH = 12 (dashed line).

solutions under different pH conditions. At pH 1, the most prominent band in the absorption spectrum is centered at 406 nm with a $\Delta\nu_{1/2} = 20$ nm. The RLS profile of the sample is rather weak and displays the expected minimum at 406 nm due to the photon loss for absorption of the radiation, pointing to the monomeric nature of the diacid form. The fluorescence emission shows two bands at 604 and 660 nm. At intermediate pH (in the range 3–7), a broadened split Soret band of moderate intensity is observable in the range 300–500 nm with maxima at 352 and 450 nm. The solutions are stable toward precipitation within a week in the presence of small quantities of cosolvent (DMSO <5% v/v). The corresponding RLS spectrum is at least 1 order of magnitude higher than that observed at lower pH and 2 orders of magnitude larger than the neat solvent. Fluorescence emission is almost totally quenched under these experimental conditions.

Figure 3 displays the progressive decrease of the 406 nm Soret band and the matching increase of the broad split Soret band in the range of pH between 1 and 4. The conversion can be also easily monitored by RLS, which shows a gradual enhancement of the scattered light intensity on increasing the pH. The profile of the absorbance at 406 nm and the RLS intensity at 500 nm exhibits a saturation behavior, which levels off at pH 4.0 and remains almost unaltered on increasing the pH of the solution to 7. A further increase of pH causes a gradual built up of a new broad Soret band at 382 nm ($\Delta\nu_{1/2} = 45$ nm), which becomes the predominant species at pH 12. The scattering profile at this final pH value is about $1/5$ with respect to the intermediate pH sample and shows a large minimum at 380 nm, almost matching the absorption feature. The fluorescence

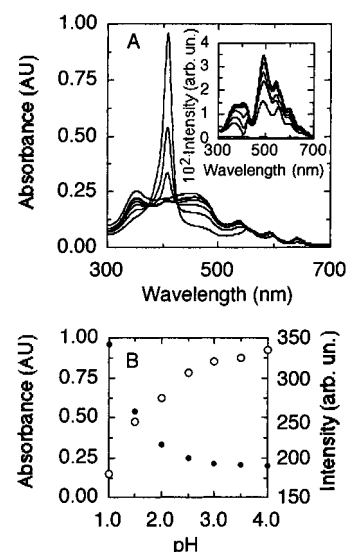


Figure 3. UV/vis (A) and RLS (inset) spectral changes of a 5 μM aqueous solution of protoporphyrin IX in the pH range 1–4 and diagram (B) of the absorbance at 406 nm (●) and of the RLS intensity at 500 nm (○) as a function of increasing pH.

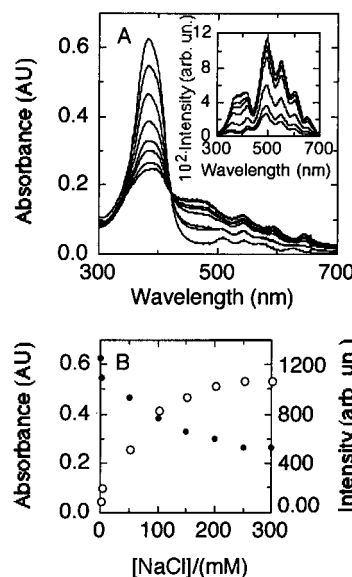


Figure 4. UV/vis (A) and RLS (inset) spectra of a 7.5 μM aqueous solution of protoporphyrin IX at various ionic strength values (pH = 12) and diagram (B) of the absorbance at 382 nm (●) and of the RLS intensity at 500 nm (○) as a function of increasing NaCl concentration.

emission is red-shifted with respect to that of the species existing at acidic pH. All of the main spectroscopic features are collected in Table 1.

An increase of ionic strength does not induce any effective change in the spectral features up to pH 7. On the contrary, the species existing at pH 12 is strongly influenced by an increase of the added NaCl concentration (Figure 4). The 382 nm band is progressively reduced in intensity, while the red region of

TABLE 1: UV/vis Absorption, Fluorescence Emission Data, and Depolarization Ratios at Resonance for Protoporphyrin IX under Different pH Conditions in Water

pH	B-band (λ , nm; $10^5\epsilon$, $\text{M}^{-1}\text{cm}^{-1}$)	Q-bands (λ , nm; $10^3\epsilon$, $\text{M}^{-1}\text{cm}^{-1}$)	emission (λ , nm)	$\rho_V(90)$
1	406 (1.7)	516 (9.6), 554 (17.2), 600 (11.6), 626 (8)	604, 660	
5	352 (0.44), 450 (0.37)	534 (21.2), 566 (15.6), 594 (14.8), 644 (12.8)	620, 676	0.14 ^b , 0.10 ^c
12	382 (0.78)	510 (13.8), 545 (12.8), 578 (12.0), 626 (10.6)	624, 684	0.15
<i>a</i>	408 (1.7)	506 (16.4), 542 (13.3), 577 (8.6), 630 (6.2)		

^a In dimethyl sulfoxide. ^b At 352 nm. ^c At 450 nm.

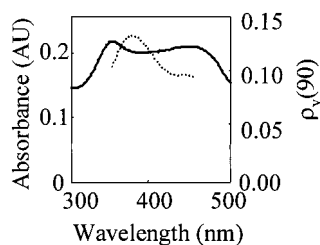


Figure 5. Dispersion profile (dotted line) of the depolarization ratio, $\rho_v(90)$, in the region of the Soret band for the aggregate at pH = 4.8 (the corresponding UV/vis spectrum is reported for comparison as full line).

the spectrum increases with an isosbestic point around 420 nm. The addition of NaCl causes a matching increase of the RLS intensity with an apparent maximum at 490 nm. The profiles of the absorbance at 382 nm and of the RLS intensity at 500 nm follow, even in this case, a saturation behavior, which levels off above 0.2 M NaCl.

Depolarized RLS has been applied to gain further insight on the structure of the species present in solution (Figure 5). The depolarization ratios measured under different experimental conditions are reported in Table 1.

Figure 6a,b shows $4 \mu\text{m} \times 4 \mu\text{m}$ wide topographic and optical images obtained by SNOM experiments. Topographic data reveal large areas of the sample that are populated by randomly oriented prolate aggregates the extension of which ranges from 0.02 to $0.05 \mu\text{m}^2$ (Figure 7). Profile analyses of the topographic images give a medium height of about 61 nm, leading to a mean volume of the aggregates of $\sim 4.42 \times 10^{-3} \mu\text{m}^3$ (Figure 8). Topographic artifacts can affect features in the optical data; however, the presence in the optical images of aggregates with higher reflectivity in areas topographically quite flat demonstrates a pure optical contrast. By using an edge resolution method of analysis,²³ we found an optical and topographic resolution of about 100 and 160 nm, respectively, with an optical contrast $C = 18\%$.

Discussion

Protoporphyrin IX can be regarded as a prototype for an amphiphilic molecule, because it possesses a large hydrophobic moiety (the porphine core) and charged hydrophilic propionate side chains. This molecule is then prone to form supramolecular assemblies such as bilayer structures.

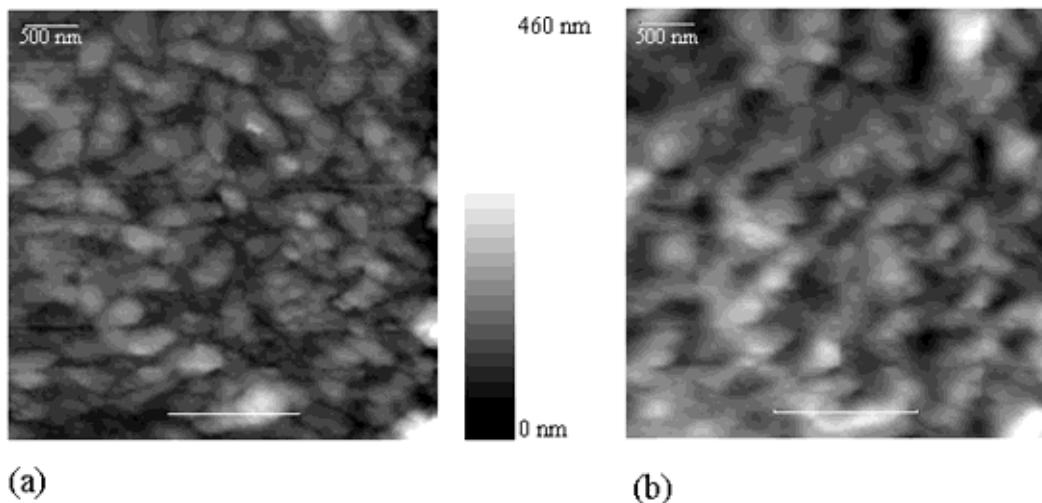


Figure 6. Topography (a) and optical SNOM images (b) of protoporphyrin IX aggregates deposited on glass substrate after evaporation from a $5 \mu\text{M}$ aqueous solution at pH 5 (128×128 points/row in a $4 \times 4 \mu\text{m}^2$ wide area; the white line at the bottom of both images refers to the profile analysis reported in Figure 8).

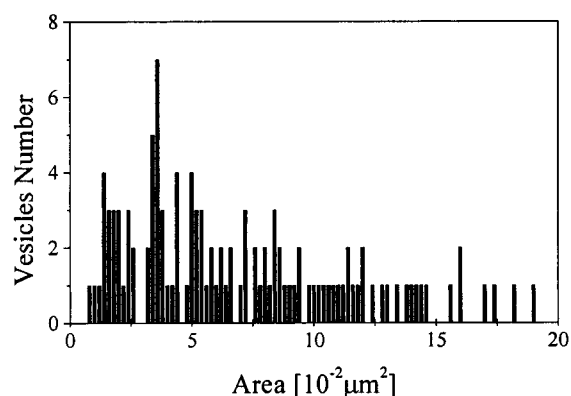


Figure 7. Histogram of the distribution of areas for the aggregates in Figure 6.

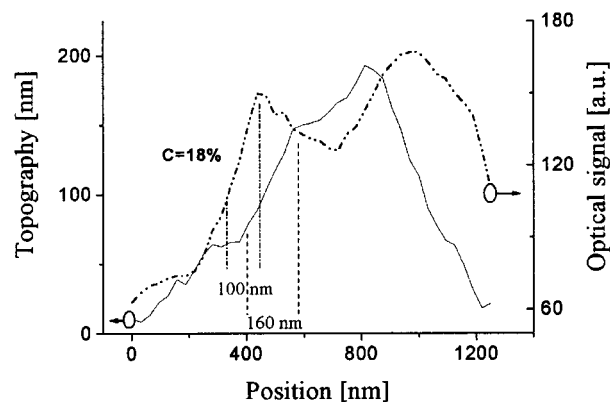


Figure 8. Topography (full line) and optical (dotted line) profile analysis of the SNOM images performed at the position indicated by the white horizontal bar in Figure 6. An optical and topographic resolution of about 100 and 160 nm, respectively, with an optical contrast $C = 18\%$ is derived.

The UV/vis spectra of protoporphyrin IX aqueous solutions evidence the presence of different species as a function of pH. At pH below 1, both the fluorescence and RLS spectra point to the existence of a nonaggregated species, which rise from the protonation of both the propionate end groups and the two nitrogen atoms of the core. This finding seems in contrast with the behavior of other water soluble porphyrins, such as the tetrakis(*p*-carboxyphenyl)porphine (TCPP)²⁴ and tetrakis(*p*-

sulfonatophenyl)porphine (TPPS),^{24–28} which under strong acidic conditions form extended J-aggregates. Several investigators have pointed out that coplanarity is a prerequisite for the initial dimerization step, together with the presence of negatively charged groups on the periphery.^{24,26} This latter condition is fully met in the case of TPPS porphyrin, which is zwitterionic even under strongly acidic conditions, leading to aggregated species that are mainly stabilized by an electrostatic attraction between the positively charged porphine core and the negatively charged sulfonate end groups. In the present case, the diacid form of protoporphyrin IX does not seem to meet this condition.

The formation of large aggregates and the consequent light scattering from the solutions on increasing pH prevent a quantitative analysis of the titration curves. Anyway, from the data in Figure 3, an apparent pK_a value of about 1.5 can be roughly estimated for the protonation of the nitrogen atoms. This value is considerably lower in comparison to pK_a values reported in the literature for the protonation of other water-soluble porphyrins.^{29,30} Indeed, both the formation of strongly aggregated species and the occurrence of specific intramolecular interactions between the propionate side chain and the inner core could be responsible for this anomalous value.

At intermediate pH (in the range 3–7), the UV/vis spectra display the presence of very broad and weak Soret bands. A peculiar behavior is the appearance of a split band with longer (450 nm) and shorter (352 nm) wavelength components. As reported in the case of other aggregated protoporphyrin IX derivatives,⁴ the fluorescence emission from these samples is substantially quenched, while the RLS spectra evidence an intense feature (at least 2 orders of magnitude with respect to the solvent) with peaks at 490, 400, and 370 nm. This latter experimental evidence is consistent with a large number of interacting chromophores in the aggregate, in agreement with previous results obtained through size-exclusion gel chromatography.^{4,10} Dynamic light scattering (DLS) experiments, assuming a spherical model for the aggregates, gave an average hydrodynamic radius of 400 nm.

The complete removal of both protons from the carboxylic end groups leads to a dianionic species. As in the case of the diacid form, the determination of a pK_a value for this process is prevented by the strong light scattering from the solutions. A value ranging between 4.8 and 5.7 has been reported for the propionate groups in hemin,³¹ while the pK_a for 3-phenylpropanoic acid is 4.37.³² In agreement with previous investigations,¹⁰ at pH above 8, the spectroscopic data suggest the presence of a face-to-face dimer. In particular, the emission features are similar to those reported for dimers of other protoporphyrin IX derivatives.⁴ The consistent blue shift in the UV/vis spectrum is in agreement with a H-type geometry according to the excitonic coupling model.^{33,34} A possible arrangement for this aggregate is a head-to-tail arrangement of the two aromatic moieties, which can maximize the stacking interactions between the porphine cores and minimize the repulsion between the charged end groups. An energy minimized structural model is reported in Figure 9.³⁵ In this model, the distance between porphyrin planes has been assumed to be 3.5–3.6 Å, which is the interplane distance theoretically calculated by Hunter and Sanders² and actually found in the X-ray crystal structures of water-soluble porphyrins.³⁰ In these investigations, it has been shown that π - π stacking interactions lead always to repulsion between the negatively charged clouds of the 22e aromatic porphine system, while σ - π interactions cause attraction between the rings. A face-to-face arrangement with a lateral offset between the planes has been proposed as one of

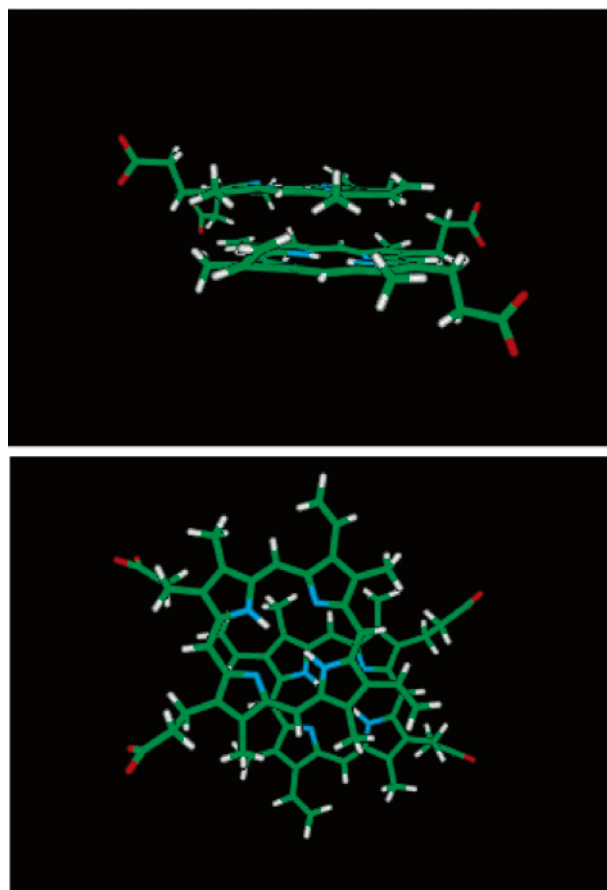


Figure 9. Molecular model for the head-to-tail H-dimer at pH 12.

the lower energy dispositions for a porphyrin dimer.² Accordingly, our molecular model evidences that about one-fourth of a porphyrin ring overlaps a corresponding adjacent area of the other porphyrin in the dimer and the charged carboxylic side chains are arranged on opposite sides. A further aggregation of the dimers can be fostered on increasing the ionic strength. Figure 4 reports a typical experiment in which the ionic strength is progressively increased in a solution containing protoporphyrin IX dimers at pH 12. The decrease of the 382 nm B-band corresponding to the dimer is matched by the parallel increase in the intensity of the light scattered from the sample. The UV/vis spectra evolve toward a final spectrum that resembles that of the aggregated species existing at intermediate pH, and the process seems to be a phase transition. The observed phenomenon is consistent with the colloidal nature of these systems. It is well-known that colloidal particles are stabilized by the DLVO (Derjaguin, Landau, Verwey, and Overbeek) potential,^{36,37} which is controlled by different parameters, such as the size of the particle, its charge, the ionic strength, and the temperature. In the case of porphyrins, the interaction potential can be varied by modulating the overall charge on the molecule or by screening the charge repulsion on increasing the ionic strength.^{38–40}

Morphological Analysis. SEM and SNOM analyses of porphyrin samples deposited on a glass surface give further insight on the morphology of these aggregated species. Both experiments exhibit the presence of aggregated structures with an average diameter of 200–500 nm, in close agreement with the DLS measurements in solution. Because of the amphiphilic character of protoporphyrin IX, it is reasonable to assume the formation of vesicles. A rough inspection of the images leads us to exclude the occurrence of a tubular bilayer arrangement.

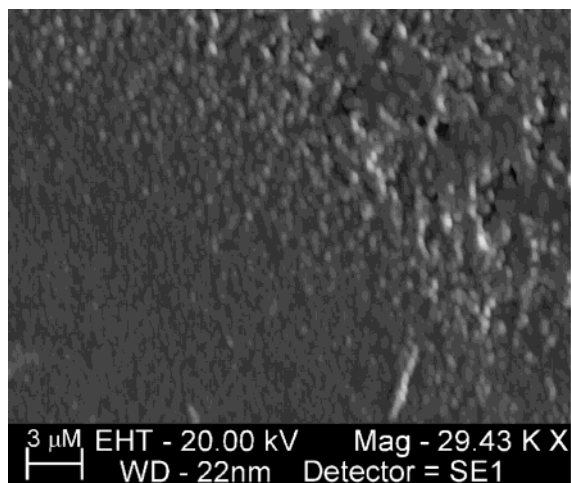


Figure 10. SEM image of protoporphyrin IX vesicles deposited on glass from aqueous solutions at pH 5 ($T = 298$ K, graphite-coated).

Simple unilamellar vesicles seem to be unlikely because, under the high-vacuum conditions of the SEM experiments, this kind of aggregate tends to be unstable because of the presence of the water pool into the inner compartment. The possibility of a multilamellar or onion-like morphology still remains open and deserves further investigation. A closer observation of the samples reveals the contemporary presence of large regions in which the vesicles collapse in a continuum layered structure.

SNOM optical data show some zones where the signal does not resemble the topographic behavior. In particular, some areas are evident in which higher reflectivity values correspond in the topographic images to an almost flat zone or to different-shaped ones. This behavior could be ascribed to a fault of the aggregation process, leading to an amorphous thin or ultrathin film, which covers the aggregates. This film produces different optical contrast and properties, as can be easily revealed by the profiles of the SNOM images.

This SNOM observation is supported by SEM analyses, which show the presence of globular aggregates, together with regions in which the structure seems to collapse in a continuum (Figure 10). Contrary to the reports of other authors, the solutions remain stable toward precipitation for at least one month, and we have not observed the absence of reproducibility of the samples.⁴ A reasonable hypothesis for the reported instability of these aggregates can be based on a kinetic effect due to the experimental protocol used to control and change the acidity of the solutions.

RLS Depolarization Ratio and Model for the Aggregate.

The theory of RLS predicts that, in contrast to the scattering cross section, which is strongly dependent on the size of the aggregate, the value of the depolarization ratio, $\rho_V(90)$, is related only to the principal values of the polarizability tensor at the resonance wavelength. As a consequence, the value of $\rho_V(90)$ can be conveniently used to gather information on the geometry of the excited state of an aggregated species.¹⁶ Assuming a parallel arrangement of the transition moments of the exciton-coupled chromophores and applying this simple model, we have calculated the slip angle α between adjacent porphyrin planes (Figure 11A). The expected range for this ratio is $1/8 \leq \rho_V(90) \leq 1/3$, with the maximum value corresponding to $\alpha = 90^\circ$ and a symmetric behavior of this parameter around $\alpha = 45^\circ$. The dimer of protoporphyrin IX at pH 12 exhibits the spectral features of a H-dimer, and the measured ratio $\rho_V(90)$ is 0.15 at 382 nm. Because of the fairly low intensity in the corresponding RLS spectra, this value could be largely due, if not entirely, to

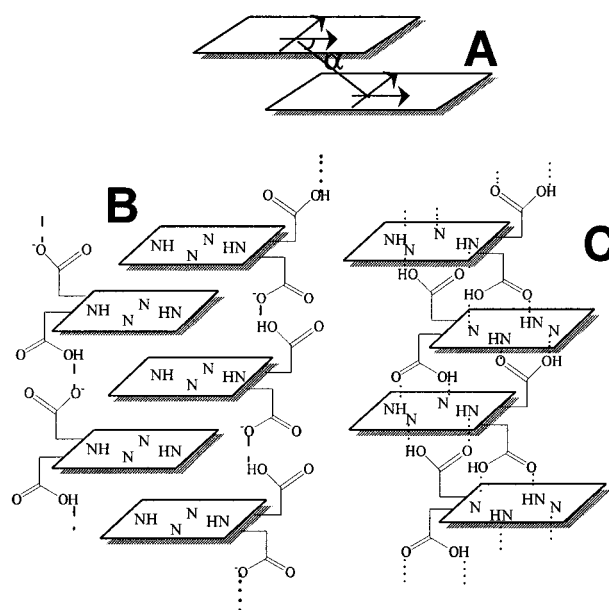


Figure 11. Slip angles (A) between porphyrins in the aggregate at pH 4.5 as derived from RLS depolarization ratio measurements ($\alpha = 38^\circ$) and the proposed hydrogen-bonding network (B,C) between adjacent dimers in the aggregates.

a nonresonant Rayleigh scattering component, which makes unreliable the application of the RLS theory. Figure 5 shows the dispersion profiles of the $\rho_V(90)$ value at the absorption feature for the higher aggregate obtained at pH 4.8. The $\rho_V(90)$ value is 0.14 at 352 nm, indicating an angle $\alpha = 38^\circ$ or 52° . In the case of bis-glycosamide derivatives of protoporphyrin IX, the origin of the apparent split Soret band has been explained by Fuhrhop et al.⁴ assuming a model based on an octamer of porphyrin units. According to this model, a face-to-face (with a lateral offset) dimer of porphyrins is stacked with another similar unit, and it is connected with a similar arrangement of porphyrins through edge-to-edge interactions. In the case of the bis-glycosamide derivatives, a further stabilization of the whole structure is achieved through a network of hydrogen bonds connecting the lateral glycosamide moieties, leading to very stable micellar fibers. In the case of protoporphyrin IX, two models can be envisaged on the basis of the experimental findings: (i) the protonated carboxylic groups are hydrogen-bonded to the two inner NH (Figure 11C) or (ii) the half neutralization of the propionic acid side chains could induce the formation of a very specific matching of donor and acceptor hydrogen-bond sites, acting in an alternate fashion between adjacent porphyrins and dimers (Figure 11B). On considering the similarity of the UV/vis spectra of protoporphyrin IX at pH 4.8 and of the bis-glycosamide derivatives, we are inclined to think that this latter could be a better model for the aggregate. Figure 12 shows a computer model of a short domain of the vesicle bilayer. This model, together with a specific role of counterions, could well apply to the aggregates formed by protoporphyrin IX at pH 12 under high ionic strength conditions. In this case, the added salt could screen the electrostatic repulsions between the four negatively charged dimers and stabilize the aggregated species through a series of specific interionic contacts.

The shorter propionic side chain, with respect to the glycosamide substituent, could be responsible for the observed instability of protoporphyrin IX aggregates and the collapse of the vesicles into a continuum membrane bilayer structure on a solid surface.

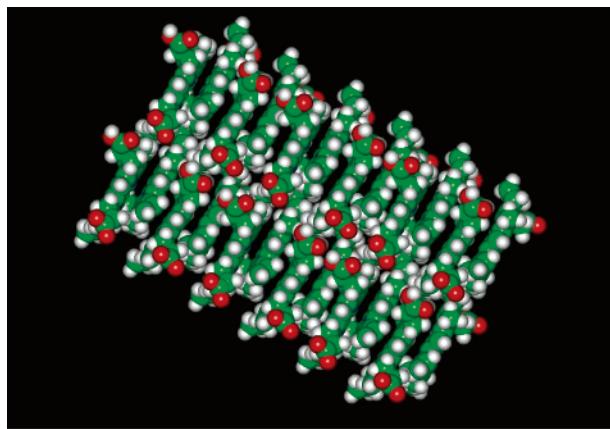


Figure 12. Molecular model for the hypothetical aggregate (24-mer).

Conclusions

According to its amphiphilic character, protoporphyrin IX in aqueous solution is able to form supramolecular assemblies. Our experimental results indicate that the previous assignment proposed by Inamura et al.¹⁰ on the nature of the species present in aqueous solutions of protoporphyrin IX was correct. The instability and low reproducibility of the samples stem from the colloidal nature of these species, which can easily undergo phase transitions. We succeeded in obtaining protoporphyrin IX vesicles stable enough to be investigated in solution and visualized through SEM and SNOM microscopy. The split Soret band observed for these aggregates has been explained on the basis of a model similar to that proposed for other protoporphyrin IX derivatives. In this case, dimers of porphyrins bind axially through π - π stacking interactions and laterally by means of strong edge-to-edge hydrophobic contacts. The whole structure is further stabilized by specific hydrogen bonding involving the carboxylic acid side chains.

Acknowledgment. We thank Dr. Maurizio Triscari and Mr. Giuseppe Sabatino for helping with SEM measurements and Dr. Norberto Micali for some light scattering experiments. This work was supported by the INFM (Progetto Sud "Nano-SNOM"), by the MURST (COFIN 1999) and by the CNR (Progetto No. 98.00539.CT11). We are grateful to the Ministero dell'Università e della Ricerca Scientifica e Tecnologica (MURST), Programmi di Ricerca Scientifica di Rilevante Interesse Nazionale, Cofinanziamento 2000-2001, and to CNR for funding this work.

References and Notes

- (1) White, W. I. In *The Porphyrins*; Dolphin, D., Ed.; Academic Press: New York, 1978; Vol. 5, Chapter 7.
- (2) Hunter, C. A.; Sanders, M. K. *J. Am. Chem. Soc.* **1990**, *112*, 5525.
- (3) Fuhrhop, J. H.; Koning, J. In *Membranes and Molecular Assemblies: The Synkinetic Approach*; Stoddart, J. F., Ed.; Monographs in Supramolecular Chemistry; The Royal Society of Chemistry: Cambridge, U.K., 1994.

- (4) Fuhrhop, J. H.; Demoulin, C.; Boettcher, C.; Koning, J.; Siggel, U. *J. Am. Chem. Soc.* **1992**, *114*, 4159.
- (5) Fuhrhop, J. H.; Bindig, U.; Siggel, U. *J. Am. Chem. Soc.* **1993**, *115*, 11036.
- (6) Fuhrhop, J. H.; Bindig, U.; Siggel, U. *J. Chem. Soc., Chem. Commun.* **1994**, 1583.
- (7) Gallagher, W. A.; Elliott, W. B. *Ann. N. Y. Acad. Sci.* **1973**, *206*, 463.
- (8) Savitski, A. P.; Vorobyova, E. V.; Berezin, I. V.; Ugarova, N. N. *J. Colloid Interface Sci.* **1981**, *84*, 175.
- (9) Inamura, I.; Isshiki, M.; Araki, T. *Bull. Chem. Soc. Jpn.* **1989**, *62*, 2413.
- (10) Inamura, I.; Uchida, K. *Bull. Chem. Soc. Jpn.* **1991**, *64*, 2005.
- (11) Maiti, N. C.; Mazumdar, S.; Periasamy, N. *J. Phys. Chem.* **1995**, *99*, 10708.
- (12) Pasternack, R. F.; Bustamante, C.; Collings, P. J.; Giannetto, A.; Gibbs, E. J. *J. Am. Chem. Soc.* **1993**, *115*, 5393.
- (13) Collings, P. J.; Gibbs, E. J.; Starr, T. E.; Vafek, O.; Yee, C.; Pomerance, L. A.; Pasternack, R. F. *J. Phys. Chem. B* **1999**, *103*, 8474.
- (14) Pasternack, R. F.; Collings, P. J. *Science* **1995**, *269*, 935.
- (15) de Paula, J. C.; Robblee, J. H.; Pasternack, R. F. *Biophys. J.* **1995**, *68*, 335.
- (16) Parkash, J.; Robblee, J. H.; Agnew, J.; Gibbs, E.; Collings, P.; Pasternack, R. F.; de Paula, J. C. *Biophys. J.* **1998**, *74*, 2089.
- (17) Lewis, A.; Isaacson, M.; Harootian, A.; Murray, A. *Ultramicroscopy* **1984**, *13*, 227.
- (18) Pohl, D. W.; Denk, W.; Lanz, M. *Appl. Phys. Lett.* **1984**, *44*, 651.
- (19) Labardi, M.; Gucciardi, P. G.; Allegrini, M. *Riv. Nuovo Cimento* **2000**, *23*, 1.
- (20) Gucciardi, P. G.; Labardi, M.; Gennai, S.; Lazzeri, F.; Allegrini, M. *Rev. Sci. Instrum.* **1997**, *68*, 3088.
- (21) Betzig, E.; Finn, P. L.; Weiner, J. S. *Appl. Phys. Lett.* **1992**, *60*, 2484.
- (22) Grober, R. D.; Harris, T. D.; Trautman, J. K.; Betzig, E. *Rev. Sci. Instrum.* **1994**, *65*, 626.
- (23) Labardi, M.; Gucciardi, P. G.; Allegrini, M.; Pelosi, C. *Appl. Phys. A* **1998**, *66*, S1-S6.
- (24) Akins, D. L.; Zhu, H.-R.; Guo, C. *J. Phys. Chem.* **1996**, *100*, 5420.
- (25) Ohno, O.; Kaizu, Y.; Kobayashi, H. *J. Chem. Phys.* **1993**, *99*, 4128.
- (26) Ribò, J. M.; Crusats, J.; Farrera, J. A.; Valero, M. L. *J. Chem. Soc., Chem. Commun.* **1994**, 681.
- (27) Maiti, N. C.; Ravikanth, M.; Mazumdar, S.; Periasamy, N. *J. Phys. Chem.* **1995**, *99*, 17192.
- (28) Rubires, R.; Crusats, J.; El-Hachemi, Z.; Jaramillo, T.; Lopez, M.; Valls, E.; Farrera, J. A.; Ribò, J. M. *New J. Chem.* **1999**, 189.
- (29) Kano, K.; Minamizono, H.; Kitae, T.; Negi, S. *J. Phys. Chem.* **1997**, *101*, 6118.
- (30) Kano, K.; Fukuda, K.; Wakami, H.; Nishiyabu, R.; Pasternack, R. F. *J. Am. Chem. Soc.* **2000**, *122*, 7494.
- (31) Smith, K. M., Ed. *Porphyrins and Metalloporphyrins*; Elsevier: Amsterdam, 1975.
- (32) *Handbook of Chemistry and Physics*, 80th ed.; Lide, D. R., Ed.; CRC: Boca Raton, FL, 1999-2000; pp 8-52.
- (33) McRae, E. G.; Kasha, M. In *Physical Processes in Radiation Biology*; Augenstein, L.; Mason, R.; Rosenberg, B., Eds.; Academic Press: New York, 1964; pp 23-42.
- (34) McRae, E. G.; Kasha, M. *J. Chem. Phys.* **1958**, *28*, 721.
- (35) Molecular models have been obtained and minimized using the molecular mechanics module (MM2 force field) with Hyperchem v5.0 (Autodesk, Inc.).
- (36) Verwey, E. J.; Overbeek, J. T. G. *Theory of the Stability of Lyophobic Colloids*; Elsevier: Amsterdam, 1948.
- (37) Derjajun, B. V.; Landau, L. *Acta Phys. Chim. Debrecina* **1941**, *14*, 633.
- (38) Mallamace, F.; Micali, N.; Trusso, S.; Monsù Scolaro, L.; Romeo, A.; Terracina, A.; Pasternack, R. F. *Phys. Rev. Lett.* **1996**, *76*, 4741.
- (39) Micali, N.; Mallamace, F.; Romeo, A.; Purrello, R.; Monsù Scolaro, L. *J. Phys. Chem. B* **2000**, *104*, 5897.
- (40) Monsù Scolaro, L.; Romeo, A.; Mallamace, F.; Micali, N.; Purrello, R. *Nuovo Cimento*, **1998**, *20D*, 2207.